Cathode Phenomena in a Low-Power Magnetoplasmadynamic Thruster

R. M. Myers,* N. Suzuki,† A. J. Kelly,‡ and R. G. Jahn§
Princeton University, Princeton, New Jersey 08544

Mass-loss and surface-temperature measurements, filter photography, and scanning electron microscope surface characterization were used to study cathode phenomena in a steady-state, self-field magnetoplasmadynamic thruster operated at power levels between 15 and 30 kW. The steady-state cathode temperature was found to be above 3000 K over most of its length, and evaporation and simple thermionic emission adequately explained the measured erosion rates and current levels. The steady-state cathode power balance was dominated by electron cooling and radiation. The arc ignition phase was found to last approximately 2 s and was characterized by spot current attachment with associated high erosion rates.

Nomenclature

E	= energy
E_i	= ionization energy
e	= electron charge
I_s	= current per cathode spot
j_e, j_i, j_t	= electron, ion, and total current densities, respectively
k	= Boltzmann constant
k_t	= thermal conductivity
$\dot{m}_{ev}$	= evaporated mass flow, g/cm^2 s
P_r, P_{ev}	= radiated and evaporation powers, respectively
p	= pressure
r_s	= cathode spot radius
S, S_b	= surface and cross-sectional areas
T_e, T_i, T_c	= electron, ion, and cathode temperatures, respectively
V	= volume
V_s	= sheath voltage
ϵ	= emissivity
μ_o	= permeability of free space
ρ	= resistivity
σ	= Stefan-Boltzmann constant
ϕ_{ef}	= effective work function

I. Introduction

THE applicability of magnetoplasmadynamic (MPD) thrusters to long duration missions will be determined in part by the cathode lifetime.[1,2] Few studies to date have presented data on cathode erosion rates. Schrade et al.[3] report a steady-state cathode mass-loss rate of 0.03 μg/C at 2500 A for 2% thoriated tungsten cathodes, which translates into a cathode lifetime of approximately 100 h (using a 10% mass-loss criterion). These measurements were performed using a nozzle-type thruster geometry, where the cathode is in a high-pressure region upstream of the throat. These are the only cathode erosion data available for steady-state, self-field MPD thrusters, though several groups have made measurements for quasisteady (~1 ms pulse duration) thrusters where the cathode remains cold (average temperature < 1000 K) during the discharge. These measurements, made using both mass-loss[4,5] and radioactive tracer[6,7] techniques, indicated average erosion rates between 5 and 15 μg/C.

In addition to the lack of an adequate cathode erosion data base, there is little theoretical understanding of erosion mechanisms. This stems in part from inadequate knowledge of cathode surface characteristics during thruster operation. Such rudimentary factors as the surface temperature and current distributions and the material characteristics have not been measured. The only surface temperature measurements published to date, made by Hugel and Kruelle[8] and King,[9] were single point measurements at the cathode tip of two very different thruster geometries under very different operating conditions. Their results were different both in magnitude and behavior, with Hugel and Kruelle reporting tip temperatures near 3200 K and King near 2200 K. Erosion rates were not recorded with either of these devices, thus making it impossible to obtain unambiguous insight into the erosion mechanisms.

Relevant cathode surface property data have been confined primarily to postrun scanning electron microscopy (SEM). Such data have shown 1 to 100-μm-diam pits on the cathode surface.[3] The current distribution has never been measured in a steady-state thruster.

This paper presents the results of an effort to directly examine cathode phenomena in a self-field MPD thruster through combined erosion rate and surface temperature measurements, filter photography, and SEM surface characterization. Following a description of the experimental apparatus and procedures in Sec. II, the results of the cathode mass-loss measurements are presented in Sec. III. The steady-state and startup phases of thruster operation are examined in more detail in Secs. IV and V, respectively. Finally, the implications of these results are discussed in Sec. VI.

II. Experimental Apparatus and Procedures

The benchmark MPD thruster geometry studied in these experiments is shown in Fig. 1. The thruster consisted of a boron nitride mass injection system and chamber enclosed in a graphite cylinder, which served as the anode conductor and thermal radiator. Propellant was injected into the chamber using a 50:50 split between annulli at the cathode base and at

Presented as Paper 88-3206 at the AIAA/ASME/SAE/ASEE 24th Joint Propulsion Conference, Boston, MA, July 11-13, 1988; received July 28, 1989; revision received June 14, 1990; accepted for publication July 16, 1990.

*Graduate Student; currently Propulsion Engineer, Sverdrup Technology, NASA Lewis Research Center, Cleveland, OH 44135.

†Undergraduate Student; currently Aerospace Technologist, Rockwell International, NASA Johnson Space Center, Houston, TX 77058.

‡Senior Research Engineer, Department of Mechanical and Aerospace Engineering.

§Professor, Department of Mechanical and Aerospace Engineering.

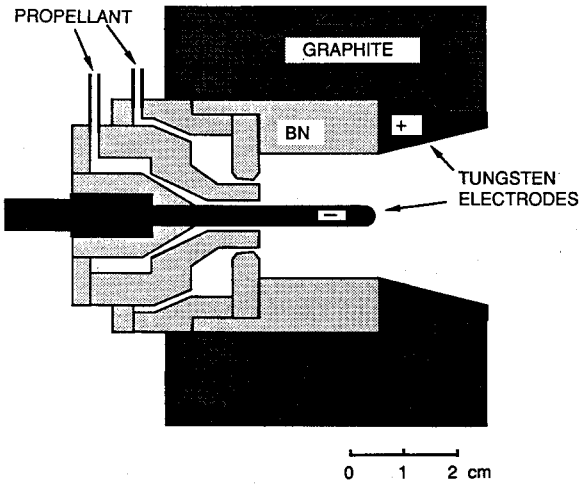

Fig. 1 Benchmark MPD thruster configuration.

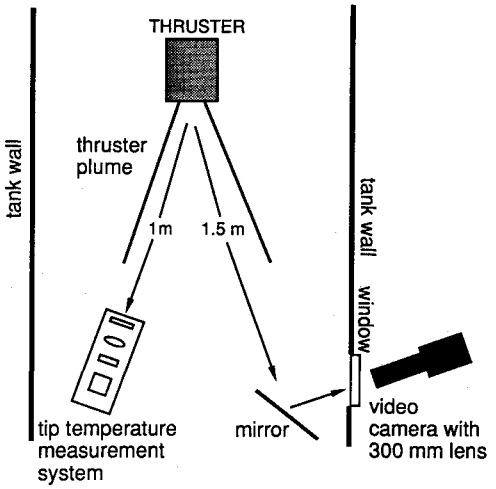

Fig. 2 Arrangement of optical diagnostics for cathode surface temperature measurements.

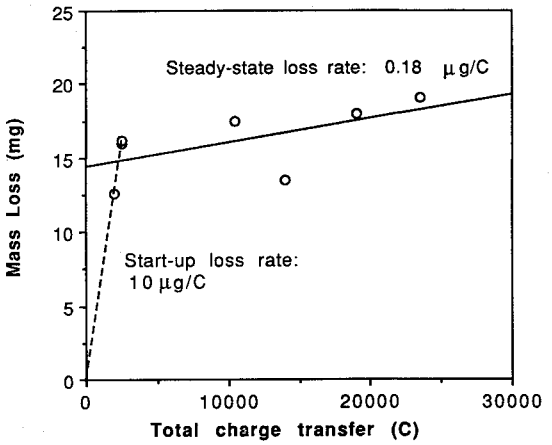

Fig. 3 Cathode mass loss as a function of total charge transfer.

the midradius between the cathode and chamber wall. The 2% thoriated tungsten cathode was 0.48 cm in diameter and extended 2.8 cm into the chamber, ending 0.3 cm before the rear edge of the anode. The second geometry, the reduced chamber radius thruster, had an identical electrode configuration to the benchmark, but the chamber area was reduced by a factor of 2 using a boron nitride insert. This insert extended the length of the insulating chamber and ended in a 45-deg flare flush with the upstream anode edge.

The thruster was mounted in a 1.5-m-diam, 5-m-long steel vacuum tank, the pressure of which was maintained below 0.07 Pa during testing. Reliable starts were obtained by discharging a 416-μF, 4000-V capacitor bank through a tungsten wire probe that was momentarily inserted into the interelectrode region. There was no correlation between the startup characteristics and either probe position or bank voltage as long as the latter was above 2500 V. The discharge triggered the main arc, which was powered by a customized 50-kW Miller welding supply (80-V open circuit, 0.5% ripple). The thruster used argon and nitrogen propellants at current levels between 600 and 1000 A. References 10 and 11 provide a more detailed description of the facility and thruster performance characteristics.

Records of total cathode mass loss, measured to ± 2 μg, permitted measurement of erosion rates as a function of the total charge transferred during a run. The test duration was varied to separate startup and steady-state mass-loss rates. Least-squares fits to these data yield the erosion rates.

Two nonintrusive optical techniques were developed to measure cathode surface temperature. The first[12] employed a simple lens, infrared long-pass filter (Corning 7-56, cutoff below 0.8 μm) and silicon photodiode (TIL81) combination to monitor the cathode tip temperature of the benchmark thruster. Spatial resolution of this system was 2 mm. The second, which permitted measurement of the entire cathode surface temperature distribution, consisted of an Ikegami ITC-400 monochrome video camera with vidicon pickup tube in conjunction with a 546.1 nm, 10.0 nm bandpass interference filter, and neutral density filters appropriate for the temperature range of interest. Video camera data were recorded on tape and analyzed using an AT&T Targa M8 frame grabber and Media Cybernetics Image-Pro software on an AT&T 6300 computer. A 300-mm focal length lens provided a spatial resolution of 0.3 mm. The interference filter was chosen to lie in a spectral region with little plasma emission. Line absorption was shown to have little influence on the measurements due to the wide bandpass of the filter, and inverse bremsstrahlung was neglected because of the low densities of the interelectrode and plume plasmas.

The arrangement of the two optical diagnostics is shown in Fig. 2. Both systems were precalibrated (to obtain brightness temperatures) using a tungsten ribbon lamp mounted at the cathode position. The calibrations indicated a measurement accuracy of ± 50 K. The conversion of these data to true temperature required knowledge of the surface emissivity,[13] which is a function of surface roughness, composition, temperature, and spectral range. For these experiments, the cathode emissivity was directly measured by drilling a 1-mm-diam, 3.96-mm-deep hole in the cathode tip, the emissivity of which was calculated to be 0.93. The hole emissivity was calculated from its length-to-diameter ratio and known characteristics of such cavities.[14] The tungsten surface emissivity was obtained by comparing the emitted intensities inside and around the hole during a run. This test showed that the emissivity was approximately 0.4. This value is slightly below that for smooth, pure tungsten (0.44) at the same wavelength and temperature.[15] There were insufficient data in the present study to establish the temperature dependence of the emissivity.

III. Cathode Erosion Rates

Cathode mass-loss measurements are plotted against integrated charge transfer in Fig. 3. For these tests, the run duration was between 3 and 30 s and the current levels and mass-flow rates were between 700 and 900 A and 12 and 15 mg/s, respectively. The temperature measurements revealed that the cathode approached an equilibrium temperature distribution ~ 2 s after the initial breakdown. Note that after the startup phase (the first ~ 1000°C) the measured erosion rate dropped off to 0.18 μg/C. Insufficient data were available to permit evaluation of the influence of the propellant, mass flow rate, or geometry on the erosion rate. Although the steady-state erosion rate in the present study was higher than that mea-

sured by Schrade et al.[3] (0.03 μg/C) for a nozzle-type thruster run at ~ 200 kW, the startup mass loss was very close to their measurements for comparable initial current levels (600–800 A). The observed difference in steady-state erosion rates may be due to the higher pressure surrounding the cathode of Schrade et al.'s device, which would enhance backscattering of ejected cathode material. The thruster chamber pressure in Ref. 3 is within the range at which the erosion rates of copper cathodes have been shown to depend strongly on ambient argon pressure.[16] This effect is further discussed in the next section. In addition, the fact that the short test duration of our runs compared to Schrade et al.'s increased the statistical influence of the startup phase for which the data were highly scattered. The agreement between the startup erosion rates is discussed in Sec. V.

The startup erosion rate shown in Fig. 3 is two orders-of-magnitude higher than that for the steady phase. Startup erosion effects are, however, of less consequence than the steady-state erosion due to the long required life. For the present data, the charge transfer after which the steady-state and startup mass losses are equal is 5×10^4 C. Thus, for a current level of 1000 A, only 50 s would elapse before the steady-state erosion dominated any startup mass loss. This same calculation for Schrade et al.'s measurements yields 330 s (5.5 min). Both of these results show that for the lengthy missions currently being contemplated, with burning times of at least several days, the steady-state mass loss limits cathode lifetime.

IV. Steady-State Phase

Figures 4 and 5 show steady cathode surface temperature distributions obtained at several current levels during operation of the reduced radius chamber geometry using nitrogen propellant at two mass flow rates. Error bars reflect uncertainty in brightness temperature and measurement repeatability; it was not possible to quantify the emissivity error. Temperature data were obtained from the cathode tip to within the mass injection annulus (tip temperature data are presented separately). For all cases, the temperature increased from approximately 2600 K at the backplate to a peak above 3200 K at the cathode midpoint and then fell to about 2600 K at the tip. The temperature increased slightly with the current level.

From these data, the thermionic current density j_{th} was calculated using Richardson's relation[17]

$$j_{th} = AT_c^2 \exp\left(\frac{-\phi_{ef}}{kT_c}\right) \quad (1)$$

where $A = 70$ A/cm^{2}K^2 and ϕ_{ef} is the effective work function, defined as the material work function minus a correction due to the Schottky effect. Two values for the effective work function, $\phi_{ef} = 3.5$ or 4.5 eV,[18] were used to examine parametrically the influence of the Schottky effect, though it was not explicitly included in the calculations. In addition, axial variations of the work function were assumed to be negligible. Although the cathode was fabricated from 2% thoriated tungsten having a work function of approximately 3.3 eV,[18] at the observed temperatures, the thorium will rapidly evaporate from the surface.

Schneider[19] shows that above 1800 K thorium evaporates from the surface more rapidly than it is replaced by diffusion from the interior, with thorium depletion occurring over a period of seconds for temperatures above 2000 K. It is therefore expected that 4.5 eV is a more realistic estimate of the cathode material work function. Typical results (for the low mass flow run) are shown in Fig. 6, where it is seen that the current density is > 150 A/cm^2 for most of the cathode at the highest thruster current level. The cathode tip and base do not contribute significantly to current emission.

The total thermionic current was calculated for each curve by numerically integrating these results over the cathode surface (assuming azimuthal symmetry and a smooth surface). Table 1 presents the calculation for total thermionic currents and the measured total thruster currents. It is evident that the two values used for the effective work function span the correct one. Although in most cases the calculated currents for $\phi_{ef} = 4.5$ eV are substantially below the measured currents, the agreement between the two is adequate considering the exponential dependence of the current on temperature. In addition, the surface roughness caused by spot attachment during the startup phase (see Sec. V) could have more than doubled the cathode surface area. This would bring the results for $\phi_{ef} = 4.5$ eV into closer agreement with the measured total

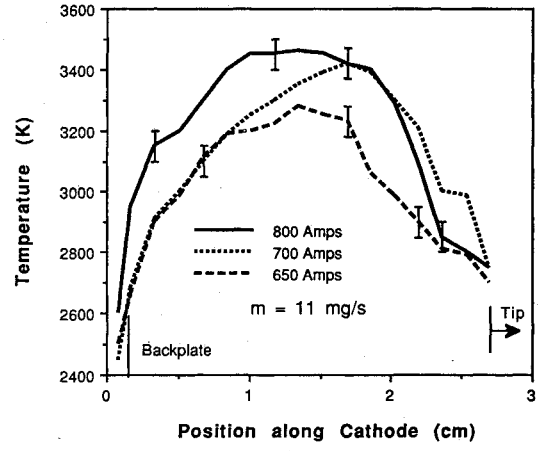

Fig. 5 Cathode temperature distributions for the reduced chamber radius thruster: nitrogen mass flow of 11 mg/s.

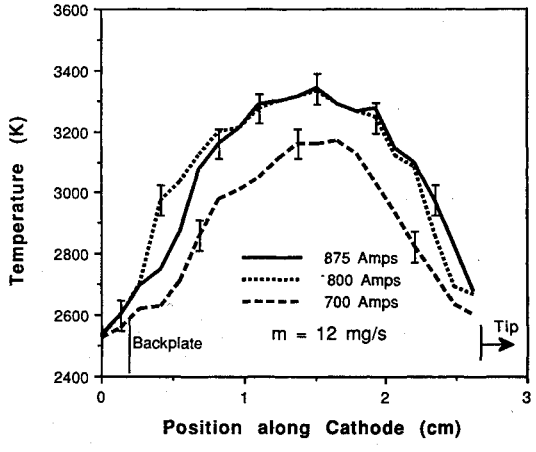

Fig. 4 Cathode temperature distributions for the reduced chamber radius thruster: nitrogen mass flow of 12 mg/s.

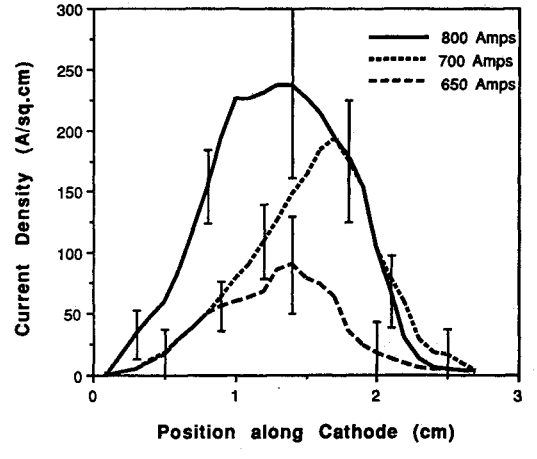

Fig. 6 Thermionic current distribution for the measured temperatures: nitrogen mass flow of 11 mg/s; $\phi_{ef} = 4.5$ eV, $A = 70$ A/cm^2.

Table 1 Comparison of measured and calculated total thermionic currents

Mass flow, mg/s	Measured current, A	$j_{th}(\phi_{ef}=3.5$ eV)	$j_{th}(\phi_{ef}=4.5$ eV)
11	800	15,000	470
	700	9,400	280
	650	5,600	150
12	875	6,600	180
	805	6,700	190
	800	8,000	230
	700	3,000	67

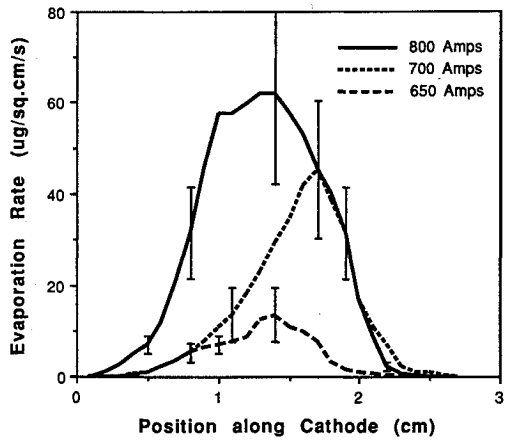

Fig. 7 Evaporation rate distribution for the measured temperatures: nitrogen mass flow of 11 mg/s.

currents. The requirement for an ion current to provide input power to the cathode and the above calculations indicate that thermionic emission with a work function of 4.5 V adequately explains cathode current conduction. Further evidence for using this work function is given later. Nevertheless, it should be noted that a double sheath over the cathode[20,21] would reduce the thermionic current for $\phi_{ef} = 3.5$ eV to more reasonable levels.

The net tungsten evaporation rate is equal to the difference between the evaporation rate in a vacuum and the redeposition rate. Rieck[18] gives an empirical relation for the evaporation rate of pure tungsten in a vacuum:

$$\dot{m}_{ev} = 10^{(7.5 - 40500/T)} \tag{2}$$

which is solely a function of temperature. Redeposition of tungsten occurs via a variety of mechanisms: simple condensation due to increased vapor pressure above the surface, backscattering via collisions with propellant atoms, and electric forces on tungsten atoms if they are ionized. The magnitudes of these processes were estimated from the appropriate mean-free paths of the tungsten atoms emerging from the cathode. The mean-free path for elastic collisions between propellant and tungsten atoms was estimated as 0.2 m using simple kinetic theory.[22] This value is an order of magnitude greater than the distance between the cathode and the relatively cool chamber wall. This result indicates that both backscattering and simple recondensation can be neglected because the tungsten atoms will move straight across the chamber. The electron-tungsten ionization mean-free path was estimated using Drawin's cross section for single step ionization[23] and an electron temperature and density of 1 eV and 10^{13} cm^{-3}. These values were measured at the exit plane.[11] These calculations yielded an ionization mean-free path of 0.8 m, or 80 times the chamber radius. It appears from these results that, for these operating conditions, redeposition does not play a significant role in establishing the cathode mass loss rate. This result is corroborated by the observation of substantial tungsten deposits on the chamber wall. In contrast, chamber pressure measurements at Stuttgart[24] indicate that for Schrade et al.'s device the corresponding mean-free paths are between two and three orders of magnitude smaller than those calculated for the device studied here, so that all the redeposition mechanisms may play a role in their thruster. This difference may explain the observed discrepancy in the steady-state erosion rates discussed in Sec. III.

Table 2 Total cathode evaporation rates calculated from measured temperatures using Rieck's relation (measured value is 0.18 μg/C)

Mass flow, mg/s	Current, A	Evaporation rate, μg/C
11.5	800	0.13
	700	0.08
	650	0.03
12.0	875	0.03
	805	0.03
	800	0.05
	700	0.01

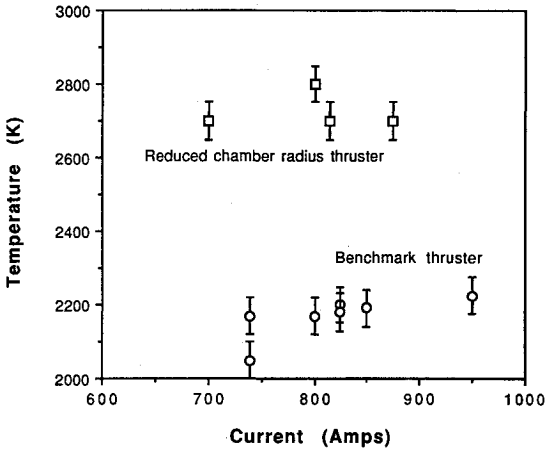

Fig. 8 Cathode tip temperatures for the two thruster geometries.

The temperatures presented earlier yield the local evaporation rates shown in Fig. 7. It is clear that the central region loses mass much more rapidly than do the cathode base or tip during the steady-state phase of operation. These local values were integrated to obtain total evaporation rates, with the results shown in Table 2. For all but one case, the evaporation rate is within a factor of 3 of the measured rate. This agreement is adequate considering the exponential dependence of evaporation rate on surface temperature, the uncertainties in the constants used in the evaporation equation, and the surface area considerations discussed earlier.

Figure 8 shows a comparison of the tip temperatures for the benchmark and reduced radius chamber thrusters. The cathode tip was cooler (by ~600 K) with the benchmark geometry. The lower temperature might be due in part to changes in the radiation balance at the cathode. The net radiative power loss from the cathode is the difference between the emitted power and the power reflected back to the cathode from the chamber walls. Reducing the chamber radius reduces the solid angle subtended by the exit plane for all chamber surfaces and increases reflection back to the cathode. An examination of the cathode power balance showed that the cathode temperature must increase for the smaller chamber radius if the sheath voltage and ion temperature remain constant.

The global cathode energy balance can be written as[25]

$$P_{r_{in}} + \int_s j_i \left(V_s + \frac{5kT_i}{2e} \right) dS + \int_s j_i (E_i - \phi)\, dS + \int_v j_t^2 \rho\, dV = \int_s \left(j_{th}\phi + \epsilon\sigma T_c^4 \right) dS + \int_{S_b} k_c \frac{dT_c}{dx}\, dS_b + P_{ev} + P_{r_{out}} \quad (3)$$

where terms on the left side represent processes adding power to the cathode and those on the right are power-loss terms. The measurements presented in previous sections permit evaluation of all of the terms on the right side of this equation, thus providing insight into the required power input.

Electron cooling power was calculated by multiplying the calculated thermionic emission current (Table 1) and the effective work function. Only results for $\phi_{ef} = 4.5$ eV are shown; results for $\phi_{ef} = 3.5$ eV indicated that for that value all thruster input power had to be deposited into the cathode to maintain its temperature against the electron cooling loss. Figure 9 shows the radiated power density as a function of position along the cathode calculated from the Stefan-Boltzmann equation using the measured cathode emissivity. The total radiated power was obtained by numerical integration of these data. The net cathode heat loss due to conduction was evaluated using the one-dimensional conduction equation (neglecting radial temperature gradients) with a linear least-squares fit to the temperature in the base region. The results of the electron cooling and conductive and radiative power loss calculations are summarized in Table 3. The cathode lost between 1 and 3 kW via these processes. The power required to evaporate a solid is given by the product of the rate of material evaporation and the vaporization energy (398 kJ/g for tungsten[18]). Using the measured steady-state erosion rates and assuming the mass loss to be due to evaporation, this yielded a power loss due to erosion of 50 W at 700 A, a small value compared to the electron cooling and radiation terms calculated earlier.

V. Startup Phase

The large difference in erosion rates between the startup and steady phases of thruster operation resulted from changes in the form of the cathode current attachment. During the first 0.4 s, the cathode was covered with rapidly moving bright spots. Between 0.4 and ~ 1.5 s (depending on initial current level), these spots were replaced by a diffuse cathode attachment, the transition behavior depending on the propellant. Figures 10 and 11 show the cathode radiant intensity distribution at various times during the startup transient for tests using argon and nitrogen propellants. The startup currents listed refer to the initial current setting for the test. The directly measured intensity is shown because the trends are more evident than with the reduced data (temperature). The data clearly show that with argon propellant the cathode heats up from the base forward, approaching an equilibrium temperature distribution after ~ 2 s. This transient duration was shorter with nitrogen propellant (Fig. 11), and the temperature peaked further forward. At no point during the transient was the bulk temperature high enough for thermionic current to be a significant fraction of the total current.

Figure 12 shows a typical current trace for the startup phase. The current level increases rapidly to 780 A at breakdown and stabilizes to 850 A after 2 s, whereas the voltage trace is quite noisy for the first 0.8 s, becomes smooth, and then falls by approximately 4 V before reaching a steady value after 1.6 s. The noise and high voltage observed during the first 2 s of operation are similar to phenomena observed for vacuum arcs. Daalder[26] ascribes this noise to the formation and extinction of current attachment spots, and the high voltage to current conduction through the molten (high resistivity) tungsten within the spots. Using the resistivity of molten tungsten[27] (1.4×10^{-6} Ωm), the cathode spot diameter, and the current per spot (measured by Daalder to be approximately 100 A for tungsten), and assuming the depth of the liquid layer to be comparable to the spot diameter, the magnitude of the voltage drop through the molten tungsten is estimated to be 3.5 V, which compares favorably with the observed 4 V change in voltage when the bulk cathode temper-

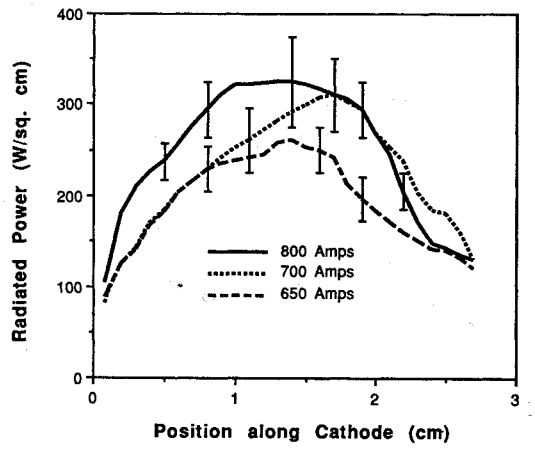

Fig. 9 Radiated power intensity for the measured temperatures, grey body with emissivity of 0.4; nitrogen mass flow of 11 mg/s.

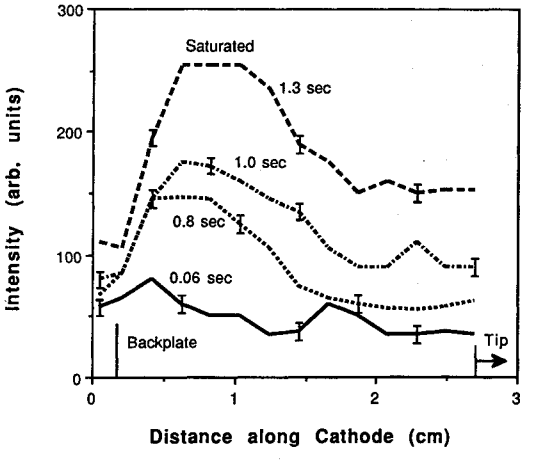

Fig. 10 Cathode radiant intensity distribution during the startup phase: argon propellant, startup current of 540 A.

Table 3 Cathode power losses calculated from temperature measurements and calculated thermionic current

Mass flow, mg/s	Current, A	$j_{th}\phi_{ef}$, W	Radiation, W	Conduction, W
11.5	800	2100	1000	120
	700	1300	880	150
	650	660	780	160
12.0	875	810	830	60
	805	860	840	160
	800	1000	860	140
	700	310	670	79

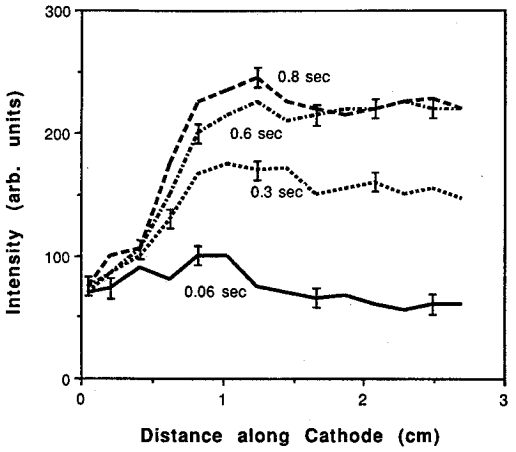

Fig. 11 Cathode radiant intensity distribution during the startup phase: nitrogen propellant, startup current of 450 A.

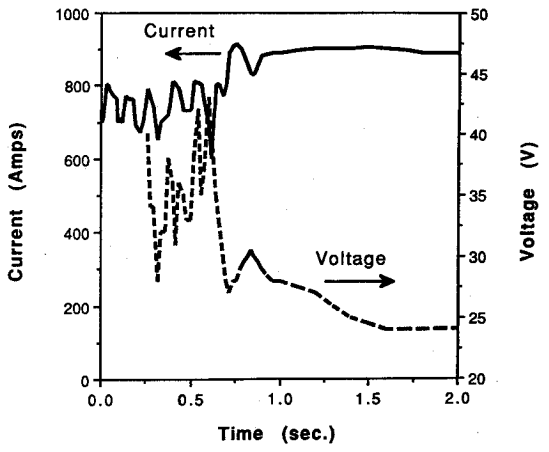

Fig. 12 Typical current and voltage traces during the startup phase.

ature becomes sufficiently high for thermionic emission. Thus, although there is no direct evidence to link the startup voltage characteristics with spot current attachment, the temporal correlation of the noise and high voltage with the cathode temperature transient lends credence to this argument.

The highly nonuniform attachment during startup resulted in severe pitting of the cathode surface. Scanning electron photomicrographs taken at several axial locations on the cathode after a single 15-s test showed that the cathode base was covered with 100-μm-diam hemispherical pits and showed evidence of melting.[28] The pits were only 10–20 μm in diameter on the cathode tip and there was no evidence of gross melting. After 61 tests, the spot size gradient was less clear due to the overlapping of many pits, though it was still evident that the surface structures tended to be larger near the base. These trends are similar to those observed in high-power quasisteady thrusters at Princeton,[29] but they are in contrast to those observed by Schrade et al.,[30] who reported larger pits near the cathode tip than at the base. The cause of the surface erosion trend observed in this study was that the initial arc breakdown occurred at the cathode base: video records of this phase showed a strong concentration of spots in this region during breakdown. This phenomenon subjects the cathode base to the effects of spot emission for a longer period of time than the cathode tip. Consequently, there is more superpositioning of molten spots at the base, with a resulting increase in the average spot size. The differences with the observations of Schrade et al.[30] are most likely due to the nozzle-type geometry of their device.

The agreement between the startup erosion rates reported here and those measured by Schrade et al.[30] is most likely due to the high pressures surrounding the current attachment spots. An estimate of this pressure is obtained by calculating the magnetic pressure above the spot[26]

$$p = \frac{\mu_o}{8\pi^2}\left(\frac{I_s}{r_s}\right)^2 \tag{4}$$

which for a spot diameter of 50 μm and a spot current of 100 A, yields a pressure of 0.6 atm. It is clear that the chamber pressure must be comparable to this value if the startup erosion rate is to become sensitive to this parameter. Neither the thrusters studied in this work nor those in Ref. 30 have chamber pressures approaching this value.

The change in current attachment modes from the startup to steady-state phases of cathode operation appears to impact the cathode power balance during these phases. The voltage drop across a current attachment spot was estimated to be approximately 4 V, which for a current level of 700 A, yields an input power of 2.8 kW. Although some of this power is ejected with the molten cathode material, a fraction will be conducted into the cathode. For the given cathode mass and observed startup transient duration (~ 2 s), only 50% of this power must be deposited into the cathode to explain the observed behavior. It is thus likely that the dominant power input term during the initial transient is joule heating in the current attachment spots. This is also true of vacuum arcs.[26]

VI. Summary and Conclusions

The cathode surface temperature measurements showed that evaporation and pure thermionic emission adequately explained the steady-state erosion rates and current levels observed in the present study: there was no need to invoke the presence of local hot spots[3,30] or sputtering.[9] Cathode temperatures were over 3000 K for most of its length, values for which any thorium on the surface would be rapidly depleted, leaving a pure tungsten surface with a work function of 4.5 eV. It appears that the Schottky effect did not play a dominant role for the devices and operating conditions studied here. Estimates of tungsten atom mean-free path in the chamber indicate that redeposition did not influence the cathode mass-loss rate and appear to explain the erosion rate differences between these results and those measured by Schrade et al.[3] The steady-state cathode power loss was dominated by electron cooling and radiation with a total power loss of between 1 and 3 kW. The startup transient was characterized by spot mode current attachment with an associated high erosion rate of 10 μg/C. The current attachment became diffuse once a steady temperature distribution was achieved, and the erosion rate dropped to 0.18 μg/C. Ohmic heating in the current attachment spots appeared to play a major role in the cathode startup transient.

The measured steady-state cathode erosion rate indicated a cathode lifetime of approximately 2 h, clearly too low for these thrusters to be of practical use in long-duration missions. The high sensitivity of the current density to the effective cathode work function indicates that future work should concentrate on reducing its value. This would permit operation at substantially lower surface temperatures and correspondingly lower erosion rates.

Acknowledgments

This research was supported, in part, by NASA Contract 954997 and grants from Rocket Research, Inc., Hercules Aerospace Company, and the U.S. Department of Energy Plasma Physics Laboratory, Princeton, New Jersey.

References

[1]Sovey, J., and Manteneiks, M., "Performance and Lifetime Assessment of MPD Arc Thruster Technology," *Journal of Propulsion and Power,* Vol. 7, No. 1, 1991, pp. 71–83.

[2]Buhler, R., "Plasma Propulsion for Near Earth Missions of Large Space Structures," Final Rept., Institute für Raumfahrtsysteme,

Univ. of Stuttgart, Stuttgart, Germany, May 1984.

[3]Schrade, H., Auweter-Kurtz, M., and Kurtz, H., "Cathode Erosion Studies on MPD Thrusters," AIAA Paper 85-2019, Oct. 1985.

[4]Shimuzu, Y., Kuriki, K., Morimoto, S., Suzuki, H., Uematsu, K., Enya, S., and Takiyama, T., "Endurance Test of MPD Arcjet Discharge Chamber," *Proceedings of the JSASS/AIAA/DGLR 17th International Electric Propulsion Conference,* IEPC 84-29, July 1984.

[5]Yoshikawa, T., Kagaya, Y., and Kuriki, K., "Thrust and Efficiency of the K-III MPD Thruster," *Journal of Spacecraft and Rockets,* Vol. 21, No. 5, 1984, pp. 481–487.

[6]Polk, J. E., Kelly, A., and Jahn, R., "MPD Thruster Erosion Research," AIAA Paper 87-0999, May 1987.

[7]Polk, J. E., von Jakowsky, W., Kelly, A., and Jahn, R., "Measurement of MPD Thruster Erosion Using Surface Layer Activation," *Journal of Propulsion and Power,* Vol. 3, No. 1, 1987, pp. 33–38.

[8]Hugel H., and Kruelle, G., "Phanomenologie und Energiebilanz von Lichtbogenkatoden bei neidrigen Drucken and hohen Stromstarken," *Beitrage der Plasmaphysik,* Vol. 9, No. 2, 1969, pp. 87–116.

[9]King, D. Q., "MPD Thruster Erosion Research," Jet Propulsion Laboratory Annual Rept., Contract NAS7-918, JPL D-3000, Jan. 1985.

[10]Myers, R., Kelly, A., and Jahn, R., "Electrothermal-Electromagnetic Hybrid Thruster Research," AIAA Paper 87-1018, May 1987.

[11]Myers, R., Kelly, A., and Jahn, R., "Energy Deposition in Low Power Coaxial Plasma Thrusters," International Electric Propulsion Conference, Paper 88-024, Oct. 1988.

[12]Suzuki, N., and Myers, R., "Electric Propulsion Laboratory Progress Report," Department of Mechanical and Aerospace Engineering, Princeton Univ., Princeton, NJ, Rept. 1776.10, Nov.–Dec. 1987.

[13]Griem, H., *Plasma Spectroscopy*, McGraw-Hill, New York, 1964.

[14]Quin, T., *Temperature,* Academic Press, New York, 1982.

[15]Svet, Y., *Thermal Radiation,* Consultants Bureau of New York, New York, 1965.

[16]Meunier, J., and Drouet, M., "Experimental Study of the Effect of Gas Pressure on Arc Cathode Erosion and Redeposition in He, Ar, and SF_6 from Vacuum to Atmospheric Pressure," *IEEE Transactions on Plasma Science,* Vol. PS-15, No. 5, 1987, pp. 515–519.

[17]Wagener, P., *The Oxide-Coated Cathode,* Vol. II, Chapman and Hall, London, 1951.

[18]Rieck, G., *Tungsten and its Compounds,* Pergamon, New York, 1967.

[19]Schneider, P., "Thermionic Emission of Thoriated Tungsten," *Journal of Chemical Physics,* Vol. 28, No. 4, 1958, pp. 675–682.

[20]Crawford, F., and Canara, A., "Structure of the Double Sheath in a Hot Cathode Plasma," *Journal of Applied Physics,* Vol. 36, No. 10, 1965, pp. 3135–3141.

[21]Prewett, P., and Allen, J., "The Double Sheath Associated with a Hot Cathode," Proceedings of the Royal Society of London A, 348, 435, 1976.

[22]Vincenti, W., and Kruger, C., *Introduction to Physical Gas Dynamics,* Krieger, 1986.

[23]Drawin, H., "Collision and Transport Cross-Sections," EUR-CEA-FC-383, March 1966.

[24]Merke, W., Auweter-Kurtz, M., and Kurtz, H., "Nozzle Type MPD Thruster Experimental Investigations," *Proceedings of the 20th International Electric Propulsion Conference,* IEPC 88-028, Oct. 1988.

[25]Ecker, G., "Electrode Components of the Arc Discharge," Eregbn. der Exact. Naturw., Vol. 33, 1961, p. 1.

[26]Daalder, J., "Cathode Erosion of Metal Vapor Arcs in Vacuum," Ph.D. Dissertation, T. H. Eindhoven, The Netherlands, June 1978.

[27]Seydel, U., and Fucke, W., "Electrical Resistivity of Liquid Ti, Mo and W," *Journal of Physics F:Metal Physics,* Vol. 10, 1980, pp. L203–L206, June 1980.

[28]Myers, R., "Energy Deposition in Low Power Coaxial Plasma Thrusters," Ph.D. Dissertation, Princeton University, Princeton, NJ, June 1989.

[29]Caswell, R., and Charlton, K., "Kerr-Cell Photography and SEM Studies of Tungsten Cathode Erosion in an MPD Thruster," Undergraduate Thesis, Dept. of Mechanical and Aerospace Engineering, Princeton University, Princeton, NJ, June 1988.

[30]Schrade, H., Auweter-Kurtz, M., and Kurtz, H., "Cathode Phenomena in Plasma Thrusters," AIAA Paper 87-1096, May 1987.